A two-scale blockage correction for an array of tidal turbines

Daniel Dehtyriov, Christopher R. Vogel, and Richard H. J. Willden

***Abstract*—This work presents an analytical blockage correction for co-planar arrays of tidal turbines based on two-scale momentum theory. The study aims to address the issue of correcting blockage effects for arrays where constructive interference between turbines can significantly improve performance. The proposed analytical model is validated by correcting Reynolds-Averaged Navier-Stokes computations of turbine arrays across a range of realistic tip-to-tip spacings (local blockage) and channel widths (global blockage) to free-flow conditions, thereby demonstrating its validity and broad applicability. By comparing the proposed two-scale correction with a single turbine correction, the necessity of the model is highlighted. Additionally, an iterative method to apply the correction is presented. This novel correction method allows for the decoupling of local and global blockage effects, enabling the isolation and quantification of the local blockage effect observed in laboratory-scale experiments. The blockage correction will further allow for comparisons of performance between arrays , and allow for an improved understanding of how tidal turbine arrays perform *in-situ*.**

***Index Terms*—Tidal energy, Blockage correction, Axial-flow turbines, Tidal turbine fence, Two-scale momentum theory**

I. Introduction

ALTHOUGH the Lanchester-Betz [1], [2] limit provides an upper bound to the power extraction of an idealised turbine in an unconstrained flow, blockage can be used to constrain the flow to raise this theoretical limit. This has been particularly relevant in tidal channels [3], where both the sea-bed and the free surface of the sea constrain the expansion of the stream-tube which encloses the turbine area. It was shown that for even modest increases in the global blockage ratio B_G, the ratio of swept turbine area to channel cross-section area, the power coefficient can significantly exceed the Lanchester-Betz limit. Constraining the flow, therefore, provides a mechanism by which the power extraction efficiency of turbines can be significantly enhanced. Extensions of this model have included the influence of free-surface deformation (non-zero Froude numbers) [4] and the development of an updated blade element momentum theory method for tidal turbines [5].

The ratio of swept rotor area to channel cross section, represented by the global blockage ratio, is however typically very small for commercial-scale tidal energy extraction [6], and turbines often cannot be placed to cover the entire channel width due to practical constraints such as bathymetry variations or shipping lane requirements. The flow around the turbines may however be constrained by placing turbines adjacent to one another to form a turbine fence partially spanning the width of the tidal channel. By reducing the inter-turbine spacing within a fence of turbines, it has been demonstrated that the turbines operate at increased efficiencies for even for small global blockage ratios [7]. This phenomenon is referred to as the constructive interference effect.

Fences consisting of multiple turbines placed side-by-side can therefore make use of this constructive interference, or local blockage effect, to raise the energy extraction efficiency of the fence above that of the Lanchester-Betz limit, even for the case where the fence makes up a negligible proportion of the channel width. The flow problem may thus be described in terms of two scales: a local scale consisting the flow around an individual turbine and its wake, and a global scale consisting of all turbines and the flux through the tidal channel. For this two-scale problem of a long array of turbines partially spanning the width of a much wider channel (vanishing global blockage) the efficiency of energy extraction, normalised on the undisturbed kinetic energy flux, rises from the Lanchester-Betz limit of 0.593 to the partial fence limit of 0.798 [7]. Experiments on pairs of side-by-side turbines at large laboratory scale [8] have confirmed the important aspects of the underlying partial fence theory and that some of the performance benefits offered by constructive interference effects can be achieved in practice.

Experimental validation of constructive interference performance benefits in laboratory facilities are however prone to global blockage effects not seen in full-scale open channel flows due to the close proximity of flow boundaries to the body. These global blockage effects modify the thrust and power performance of the turbines, such that corrections to experimental

Part of a special issue for EWTEC 2023. Original version published in EWTEC 2023 proceedings at https://doi.org/10.36688/ewtec-2023-366.

Manuscript submitted 3 January 2025; Accepted 8 January 2025. Published 31 May 2025.

This article has been subject to single blind peer review by a minimum of two reviewers

D.D is funded by an EPSRC studentship, grant number EP/S023801/1, and R.H.J.W is supported by an EPSRC Advanced Fwlloship EP/R007322/1 and by the EPSRC Supergen ORE Hub, grant number EP/S000747/1.

Daniel Dehtyriov (e-mail: daniel.dehtyriov@maths.ox.ac.uk), Christopher R. Vogel (e-mail: christopher.vogel@eng.ox.ac.uk) and Richard H. J. Willden (e-mail: richard.willden@eng.ox.ac.uk) are affiliated with the Department of Engineering Science, University of Oxford, Oxford OX1 3PJ, U.K.

Digital Object Identifier: https://doi.org/10.36688/imej.8.101-108

curves are necessary to either translate laboratory-scale experimental results to full-scale conditions, or to calculate the expected loads and power on tidal turbines deployed in blocked-flow conditions [9], [10]. The difficulty with applying blockage corrections to turbine arrays is the non-linear interaction between local and global blockage. These two effects cannot be simply decoupled as for various turbine tip-to-tip spacings (affecting local blockage), changes in the global blockage have a different impact on turbine performance.

A number of blockage corrections have been developed for single turbines operating in blocked flow conditions. These corrections are all based on Glauert's method [11], and typically seek to describe an equivalent free-stream velocity which, in the absence of global blockage, would result in the same thrust and velocity through the turbine as in the blocked case. Thrust and power curves are then scaled non-linearly with the ratio of the experimental tank velocity and the equivalent free-stream velocity. For channel flow, the most widely used correction is a method developed by Barnsley and Wellicome [12], and introduced to the marine energy community in [13]. Various other single-turbine corrections have been proposed [14]–[17]; see [9] for detailed numerical and [10] for detailed experimental comparisons of these blockage corrections. These single-scale blockage corrections can however only account for global blockage, and simplifications for turbine arrays must currently be made based on the assumption that global and local blockage effects can be linearly decoupled [8].

This work therefore presents an analytical blockage correction for co-planar arrays of tidal turbines based on two-scale momentum theory developed for partial turbine fences [7]. The correction allows for a decoupling of the global blockage and constructive interference effects, such that the local blockage effect can be isolated and quantified. This correction is compared the Barnsley & Wellicome [12] correction for a single turbine to demonstrate the necessity of the two-scale blockage correction. Finally, Reynolds-Averaged-Navier-Stokes (RANS) computations of turbine arrays across various local and global blockage ratios are corrected using the analytical model, demonstrating its validity.

II. Theoretical model

A. Two-scale partial fence model

We start with the two-scale partial turbine fence theoretical model presented by Nishino & Willden [7]. A rectangular channel with uniform height h and width w, contains a large number n of turbine rotors with a diameter of d which are spaced with equal spacing s in a spanwise fence configuration as shown in Fig. 1. The flow through the channel is assumed to be incompressible and inviscid, and the flow far upstream of the array U_C is assumed uniform and fixed. The analysis of the flow problem assumes a separation of scales between the flow around each device and around the entire array, such that all device-scale flow

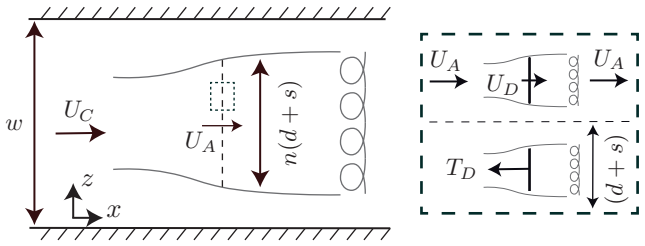

(a) Top-down view of the tidal channel, showing the global array and local device scales

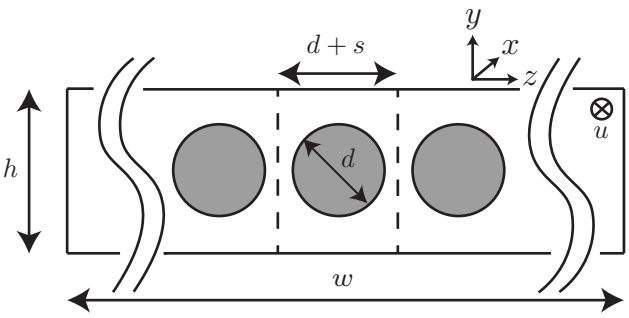

(b) Channel cross-section at the fence plane

Fig. 1. A schematic of of a tidal channel with a co-planar fence of turbines. For a given channel height h and turbine diameter d, the spacing s between each turbine defines the local blockage, and for a fixed number n of turbines, the width of the channel w, defines the global blockage. At the global array scale, the channel flow velocity U_C is reduced by the presence of the array to U_A at the fence, and recovers to U_C far downstream of the fence after wake-mixing. At the local device scale, the array velocity U_A is reduced to U_D at the discs before again recovering to U_A after local-scale wake mixing. The channel is typically significantly wider than the turbine fence.

events, including the local wake-mixing, takes place much faster than the streamtube expansion of the flow around the entire array. This allows the flow system to be solved as a combination of two coupled quasi-inviscid problems of different scales, namely the array scale and device (local) scale, see Fig. 1.

Blockage ratios for these two scales are defined. The first is an array scale blockage, which represents the array constrained by the sea-bed and sea-surface. This array scale blockage, or the ratio of representative array area to channel cross sectional area is

$$B_A = \frac{hn(d+s)}{hw} = \frac{1+s/d}{w/(nd)}. \tag{1}$$

We define the streamwise velocity at the fence U_A, and assume it to be uniform across the array. The second geometric ratio is the local (device) scale blockage, where the turbines are constrained by adjacent devices. This local scale blockage, or ratio of single turbine area to local passage cross-sectional area is

$$B_L = \frac{\pi d^2/4}{h(d+s)} = \frac{\pi}{4(h/d)(1+s/d)}. \tag{2}$$

The streamwise velocity through the turbines is denoted U_D, and is likewise assumed to be uniform across the device area. The global blockage $B_G = B_L B_A$ is then the ratio of total device area to channel cross-sectional area.

These blockage ratios define the geometry of the flow problem. The turbine operating condition is defined in terms of the thrust coefficients at each scale. The local

thrust coefficient defines the disc thrust in terms of the local inlet velocity

$$C_{TL} = \frac{T_D}{\frac{1}{2}\rho U_A^2 A_D}, \tag{3}$$

where T_D is the turbine thrust and A_D the turbine area. The array thrust (nT_D) is normalised on the array area and channel inlet velocity for the array thrust coefficient

$$C_{TA} = \frac{U_A^2}{U_C^2} B_L C_{TL} = (1-\alpha_A)^2 B_L C_{TL}, \tag{4}$$

where $(1-\alpha_A)$ is the array scale velocity induction factor. Finally, the global thrust coefficient is the total thrust (equal to the array thrust), normalised on the channel inlet velocity and total device area (nA_D)

$$C_{TG} = (1-\alpha_A)^2 C_{TL}. \tag{5}$$

Alongside the array scale velocity induction factor, we additionally define the local scale induction factor $\alpha_L = 1 - U_D/U_A$ and global induction factor $\alpha_G = 1 - U_D/U_C$, where $(1-\alpha_G) = (1-\alpha_L)(1-\alpha_A)$.

For a given geometry (blockage ratio) and turbine operating condition (thrust coefficient), we are interested in the power extraction $T_D U_D$, which similar to the thrust coefficients can be parameterised by the local $C_{PL} = C_{TL}(1-\alpha_L)$, array $C_{PA} = C_{PL} B_L (1-\alpha_A)^3$ and global $C_{PG} = C_{PL}(1-\alpha_A)^3$ power coefficients.

Conservation of mass, momentum and energy can then be solved for both local and array scales to obtain thrust coefficients in terms of velocity induction factors (see [7] for details)

$$C_{TL} = (1-\gamma_L)\frac{(1+\gamma_L) - 2B_L(1-\alpha_L)}{(1-B_L(1-\alpha_L)/\gamma_L)^2}, \tag{6}$$

$$C_{TA} = (1-\gamma_A)\frac{(1+\gamma_A) - 2B_A(1-\alpha_A)}{(1-B_A(1-\alpha_A)/\gamma_A)^2}, \tag{7}$$

where γ is the wake velocity induction factor and is related to the disc velocity induction factors by

$$1-\alpha_L = \frac{1+\gamma_L}{(1+B_L) + \sqrt{(1-B_L)^2 + B_L(1-1/\gamma_L)^2}}, \tag{8}$$

$$1-\alpha_A = \frac{1+\gamma_A}{(1+B_A) + \sqrt{(1-B_A)^2 + B_A(1-1/\gamma_A)^2}}. \tag{9}$$

The two scales are then coupled by (4) & (7), as the array thrust from both expressions must be equal.

B. Two scale blockage correction model

Blockage correction methods seek to find a relationship between the upstream velocity in a blocked flow and the equivalent upstream velocity in free-flow for which the turbine would be operating at the same conditions, i.e. the same mass flux and turbine thrust through the rotor plane. We use a prime ′ to denote the free-flow unblocked case, where we are therefore looking for the equivalent channel free-stream velocity U_C' to generate the same thrust and disc velocity through the turbines as in the original blocked case.

Setting the disc velocity and thrust to be equivalent between unblocked and blocked flow cases

$$U_D = U_C(1-\alpha_G) = U_D' = U_C'(1-\alpha_G'), \tag{10}$$

$$T_D = \frac{1}{2}\rho U_A^2 A_D C_{TL} = T_D' = \frac{1}{2}\rho U_A^2 A_D U_A'^2 C_{TL}'. \tag{11}$$

Noting that $U_A = U_C(1-\alpha_A)$ and that $(1-\alpha_G) = (1-\alpha_A)(1-\alpha_L)$ the condition on the thrust reduces to

$$\frac{C_{TL}}{(1-\alpha_L)^2} = \frac{C_{TL}'}{(1-\alpha_L')^2} \tag{12}$$

$$f(\gamma_L) = f(\gamma_L'), \tag{13}$$

where if we assume that f is an injective function (see equations 6 & 8), which must be true for the physical equations to have unique solutions, $\gamma_L = \gamma_L'$. It then follows that $\alpha_L = \alpha_L'$ and that $C_{TL} = C_{TL}'$. This result can be intuited from the fact that the function f excludes the array scale blockage B_A, which is the variable that changes between the unblocked and blocked flow equations (B_L remains the same). These identities can additionally be readily verified numerically.

Now consider the unblocked free-flow case, for which $B_A' = B_G' = 0$. Equations for the array scale variables (9), (4) and (7) reduce to

$$(1-\alpha_A') = \frac{1+\gamma_A'}{2} \tag{14}$$

$$C_{TA}' = (1-\alpha_A')^2 B_L C_{TL}' \tag{15}$$

$$C_{TA}' = (1-\gamma_A')(1+\gamma_A'). \tag{16}$$

By writing γ_A' in terms of α_A' (14), setting $C_{TL} = C_{TL}'$ (12) and equating (15) & (16), these expressions allow for a relationship between the free-flow array scale axial induction factor and the blocked flow conditions

$$4\alpha_A'(1-\alpha_A') = (1-\alpha_A')^2 B_L C_{TL} \tag{17}$$

$$(1-\alpha_A') = \frac{4}{4 + B_L C_{TL}} \tag{18}$$

Finally, we seek a relationship between the blocked and free-flow upstream channel flow velocities which, by assuming the disc velocity is the same between the two cases as in (10), can be shown to be related to the array scale induction factors by

$$\frac{U_C}{U_C'} = \frac{(1-\alpha_G')}{(1-\alpha_G)}, \tag{19}$$

$$\frac{U_C}{U_C'} = \frac{(1-\alpha_L')(1-\alpha_A')}{(1-\alpha_L)(1-\alpha_A)}, \tag{20}$$

$$\frac{U_C}{U_C'} = \frac{(1-\alpha_A')}{(1-\alpha_A)}. \tag{21}$$

Combining (18) and (21), the correction factor reduces to

$$\frac{U_C}{U_C'} = \frac{4}{4(1-\alpha_A) + B_L C_{TL}(1-\alpha_A)} \tag{22}$$

or alternatively

$$\frac{U_C}{U_C'} = \frac{(1-\alpha_A)}{(1-\alpha_A)^2 + B_L C_{TL}(1-\alpha_A)^2/4}, \tag{23}$$

$$\frac{U_C}{U_C'} = \frac{4(1-\alpha_A)}{4(1-\alpha_A)^2 + C_{TA}}. \tag{24}$$

This form of the correction factor is comparable to the Barnsley & Wellicome [12] correction, except extended from a single disc to a turbine fence partially spanning a channel by applying two-scale momentum theory. Note that the array thrust coefficient C_{TA} is a function of the local blockage ratio B_L, coupling the two scales in (24).

Equation (24) can now be used to correct for the tip-speed ratio (TSR), thrust and power coefficients:

$$\text{TSR}' = \text{TSR}\left(\frac{U_C}{U_C'}\right), \tag{25}$$

$$C_T' = C_T\left(\frac{U_C}{U_C'}\right)^2, \tag{26}$$

$$C_P' = C_P\left(\frac{U_C}{U_C'}\right)^3. \tag{27}$$

For a given recorded tip-speed ratio, thrust and power coefficient in a blocked flow (for example in a laboratory scale towing tank experiment), (24) can be used to find U_C/U_C' and (25)-(27) can then used to correct to the device operating in free-flow conditions. We note that the same formulation can be applied to consider corrections to a non-zero global blockage ratio, say for instance to estimate the performance of an array in a large tidal channel which has been tested in a towing tank, i.e., where $B_A > 0$.

C. Numerical solutions to the two-scale blockage correction

We now outline a numerical scheme which can be followed to implement the proposed blockage correction. The inputs are the array scale blockage B_A and the local blockage B_L, which can be found from (1)-(2) and depend on the channel geometry and turbine layout. Assuming turbine power P_D, thrust T_D and the free-stream velocity U_C are measured, both C_{TG} and C_{PG} are known.

By the array thrust coupling outlined in section II-A

$$C_{TG} = \left(\frac{1-\gamma_A}{B_L}\right)\left(\frac{(1+\gamma_A)-2B_A(1-\alpha_A)}{(1-B_A(1-\alpha_A)/\gamma_A)^2}\right), \tag{28}$$

where we have used (5) and where α_A is given by (9). This can be solved iteratively by a root-finding algorithm for γ_A, which can then be substituted back into (9) for $(1-\alpha_A)$. The local thrust coefficient is then $C_{TL} = C_{TG}/(1-\alpha_A)^2$, from which (6) can again be used with a root-finding method to find both γ_L and $(1-\alpha_L)$. Finally, (4) can be used to find C_{TA}. This process is illustrated diagrammatically in Figure 2 for reference.

These solutions can be substituted into (24) for the velocity correction factor, and (25)-(27) for the blockage correction factors. This procedure can then be looped over a number of inputs for the blockage corrected curves, for instance a range of turbine spacing or range of turbine thrust.

III. Numerical Method

We validate the proposed blockage correction on 3-D Reynolds-Averaged-Navier-Stokes simulations of turbine fences in channels of varying widths and realistic turbine tip-to-tip spacings.

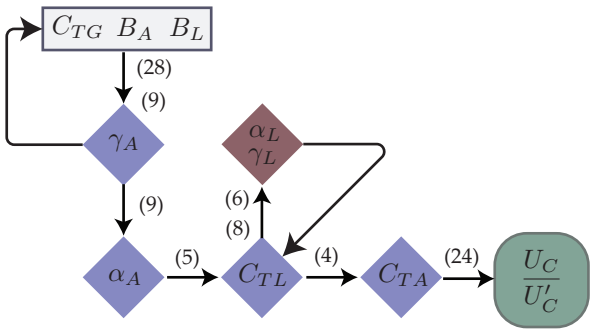

Fig. 2. Flowchart outlining the process to solve for the blockage correction, with the relevant equations which need to be solved shown. Loops imply that the respective equations need to be solved iteratively.

A. Numerical setup

Fig. 1 shows an example of the cross-section of the simulated channel. The Cartesian coordinates (x, y, z) represent the streamwise, vertical and spanwise directions. The domain boundaries are located at $-50d \leq x \leq 50d$, $0 \leq y \leq (h/d)/2$, $0 \leq z \leq (w/(nd))/2$, with the streamwise boundaries set far enough from $x = 0$ such that the boundary location does not influence the results. Uniform streamwise flow is assumed at the inlet, and zero streamwise flow gradients at the outlet. We simulate a quarter of the entire domain by setting a symmetry condition at the $z = 0$ and $y = 0$ boundaries, with the remaining boundaries set to a free-slip condition.

We consider a fence of $n = 8$ discs of diameter d, located at the centre of the channel at $x = 0$. We fix the height of the channel $h/d = 2$, and vary the local and global blockage through the disc spacing s/d and channel width $w/(nd)$ respectively.

An O-grid mesh with a minimum of 30 grid points across the diameter of each disc is used to model each disc in $y-z$ plane of the channel, with additional mesh refinement at the disc boundary. The discs thickness is taken to be $0.02d$, with axial grid refinement to ensure a minimum of 10 grid points across the disc thickness. The disc thickness and grid density are selected such that further decreases/refinement do not influence the results by over 0.5%.

The RANS equations are then solved in OpenFOAM with the Reynolds stress terms modelled using the $k-\epsilon$ viscosity model [18]. We assume an inlet turbulence intensity of $I = 0.1\%$, with the inlet turbulent kinetic energy then $k = 1.5(IU_C)^2$ and inlet kinetic energy dissipation rate $\epsilon = C_\mu^{0.75}k^{1.5}/L$, where we take $C_\mu = 0.09$ and the reference length scale as $L = 0.1d$. Changes to the inlet turbulence conditions do not affect the results as long as the inlet turbulence intensity remains relatively small. Finally, the kinematic viscosity is set to $\nu = 10^{-6}\,m^2/s$, which needs to be arbitrarily small enough such that the inertial forces dominate the viscous forces.

As demonstrated by Nishino & Willden [19], the performance of the disc fence is limited by the mixing rate, which can be controlled by variations in the turbulence model coefficient $C_{\epsilon,1}$. Following [19], we set $C_{\epsilon,1} = 1.36$ to promote stronger mixing relative to the

TABLE I
SUMMARY OF THE NUMERICAL SIMULATION CONDITIONS

Number of discs n	8
Disc thickness	$0.02d$
Disc resistance	$K(U_D^2/2)$
Turbulence model	$k-\epsilon$ [18]
I	0.1%
k	$1.5(I \cdot U_C)^2\ m^2/s^2$
C_μ	0.09
$C_{\epsilon,1}$	1.36
L	$0.1d$
ν	$10^{-6}\ m^2/s$

nominal standard case, which itself does not represent anything physically standard in terms of wake mixing of actuator discs. Similar results would however be observed under different choices (including the regular choice) of $C_{\epsilon,1}$ [19].

Disc resistance is modelled by a change in the momentum flux equal to $S_U = K(U_D^2/2)$, where U_D is the local streamwise velocity, and is added to the momentum equation by distribution over the cell volumes at the location of the discs. The disc momentum loss factor K is assumed to be uniform across the surface of all discs. We neglect rotational effects, which we assume are decoupled from the blockage effect, and can therefore be considered separately. The global axial induction factor can then be defined as $\langle \alpha_G \rangle = 1 - \langle U_D \rangle / U_C$, and the resultant disc averaged global thrust and power coefficients can then be determined by $\langle C_{TG} \rangle = K\langle U_D^2 \rangle / U_C^2$ and $\langle C_{PG} \rangle = K\langle U_D^3 \rangle / U_C^3$, where the angle brackets represent volume averaging over all discs in the fence. The numerical simulation conditions are summarised in table I, and simulations are performed over a range of K such that the peak power point is always located.

B. Numerical validation

We validate our formulation against the $n = 8$, $s/d = 0.25$, $w/(nd) = 10$ simulations presented by Nishino & Willden [19], shown in Fig. 3. Three analytical curves are shown, representing the Garrett & Cummins [3] model assuming local or global blockage for B as the lower and upper bounds respectively, and the Nishino & Willden [7] two-scale model which uses both. Across all local and global blockage ratios, the fence performance curves rest between the upper and lower bounds of the Garrett & Cummins [3] model, with the Nishino & Willden [7] model an excellent fit for the actual performance. The numerical formulation presented herein clearly matches the theoretical curve and previous numerical simulation results, giving further confidence in both the grid quality and finite volume formulation for the momentum sink.

C. Numerical results

We present results for the channel and turbine configurations in Table. II and Table. III, representing 16 simulations of varying turbine and channel configurations.

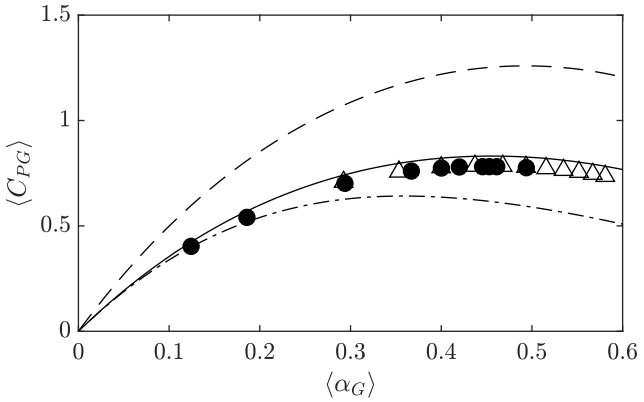

(a) Fence averaged power coefficient

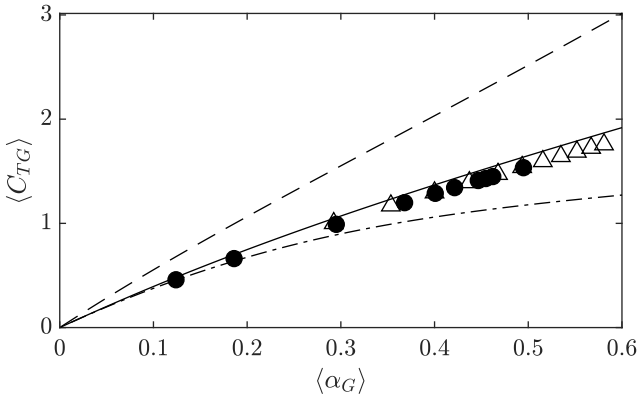

(b) Fence averaged thrust coefficient

Fig. 3. A validation study comparing numerically simulated fence averaged performance coefficients plotted against the fence averaged axial induction factor against both theoretical and published numerical results. Triangles show the results for the $s/d = 0.25$, $w/(nd) = 10$, $n = 8$ case, with the circles showing results for the same case in [19]. The dashed and dash-dot curves represent the Garrett & Cummins [3] single-scale model assuming that the blockage is global or local respectively. The solid curve represents the two-scale turbine fence model [7].

TABLE II
THE RANGE OF TIP-TO-TIP DISC SPACING CONSIDERED FOR NUMERICAL SIMULATIONS TO VALIDATE THE THEORETICAL BLOCKAGE CORRECTION. FOR ALL SIMULATIONS THE CHANNEL HEIGHT $h/d = 2$ AND NUMBER OF DISCS $n = 8$.

s/d	B_L
0.1	0.357
0.25	0.314
0.5	0.262
1.0	0.196

TABLE III
THE RANGE OF CHANNEL WIDTHS CONSIDERED FOR NUMERICAL SIMULATIONS TO VALIDATE THE THEORETICAL BLOCKAGE CORRECTION. FOR ALL SIMULATIONS THE CHANNEL HEIGHT $h/d = 2$ AND NUMBER OF DISCS $n = 8$.

$w/(nd)$	B_G
2	0.196
4	0.098
10	0.039
40	0.010

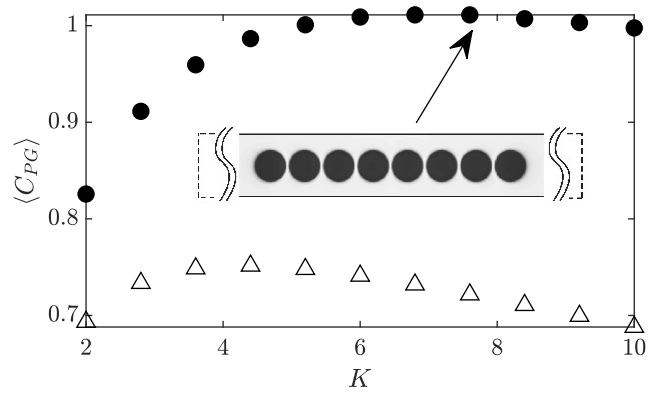

(a) Fence averaged power coefficient

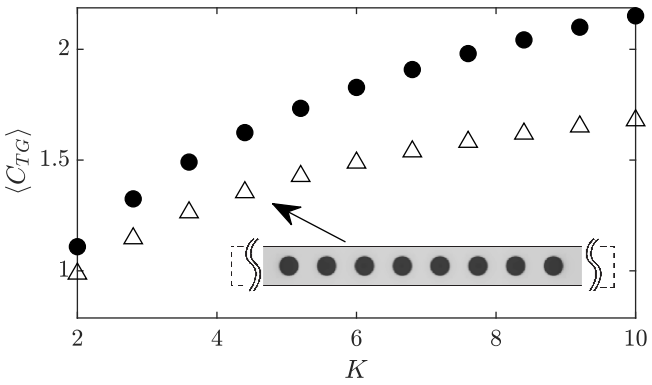

(b) Fence averaged thrust coefficient

Fig. 4. Example solutions to the numerical model, here shown for the two cases representing the largest (with circles, $s/d = 0.1$, $w/(nd) = 2$) and smallest (with triangles, $s/d = 1$, $w/(nd) = 40$) combination of local and global blockage. Fence averaged performance coefficients are plotted against the momentum loss factor K. For all simulations we assume a fixed disc number $n = 8$ discs and fixed channel height $h/d = 2$. The two insets show streamwise velocity contours at peak power, taken at an axial channel-cross section at the plane of the turbines for the two configurations.

Two example simulation results representing the lowest ($s/d = 1$, $w/(nd) = 40$) and highest ($s/d = 0.1$, $w/(nd) = 2$) blockage cases are shown in Fig. 4, with streamwise velocity contours at peak power, taken at an axial channel-cross section at the plane of the turbines for both configurations. The entire channel width is not shown, but is patently significantly smaller for the channel with larger global blockage. For all channels, the averaged thrust coefficient monotonically increases with the momentum loss factor K, and the averaged power coefficient sees a distinct maximum for $2 \leq K \leq 8$, where we note that $K = 2$ is the optimal momentum loss factor for a single disc in an unbounded flow. An increase in the global blockage always increases the peak power coefficient for a given number of discs and turbine spacing. Note that the power coefficient can, as in Fig. 4, exceed $C_{PG} = 1$, as additional energy can be extracted from the pressure drop along the channel length. For a given global blockage, however, there exists an optimal turbine spacing, or local blockage, to maximise the power coefficient. As the peak power coefficient increases for a given configuration, the required thrust to realise this peak power also increases.

Fig. 5 first demonstrates the need for a two-scale

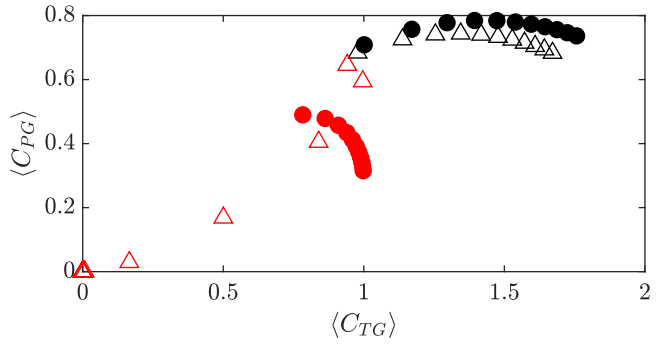

Fig. 5. A comparison of the presented blockage correction model against a widely used single-scale blockage correction model presented by Barnsley & Wellicome [12], here shown for an example case of $s/d = 0.25$, $w/(nd) = 10$. The solid black circles show the numerical results, with the triangles the corrected curve applying our model. The red triangles and circles show the corrected curves applying the single-scale model assuming that the blockage ratio is local and global respectively, demonstrating the necessity for a two-scale correction.

blockage correction by an example correction of the $s/d = 0.25$, $w/(nd) = 10$ case by comparing the widely used Barnsley & Wellicome [12] single-turbine correction to the proposed two-scale correction. Unlike the thrust and power curves in Fig. 3 for which the two-scale model is bounded by the single-scale model assuming $B = B_G$ and $B = B_L$ for upper and lower bounds respectively, the single-scale blockage correction gives inconsistent results for the turbine fence, due to the large differences in operating conditions between a turbine fence and single tidal turbine.

D. Two-scale blockage corrected simulations

We now consider correcting the blocked flow simulations by applying the proposed theoretical blockage correction to the thrust and power curves for the various channel configurations. Fig. 6 presents the results of all numerical simulations of the channel and turbine configurations presented in Table. II and Table. III, alongside the free-flow blockage corrected curves found by applying the theoretical formulation presented herein. Each subfigure represents a fixed turbine configuration, represented by a fixed tip-to-tip turbine spacing or local blockage. The range of tip-to-tip distances represent realistic turbine fence spacings. The channel width is then varied by over an order of magnitude, representing the range from laboratory scale flow testing to a near unblocked, or a near infinitely wide, channel.

The proposed blockage correction applied to the numerically simulated cases always corrects the performance curves to values slightly below the simulated lowest blockage case ($B_G = 0.01$), confirming the validity of the theoretical model. Additionally, with the blockage correction applied to all cases (including the $B_G = 0.01$ cases), the correction predicts consistent free-flow performance (for each given turbine spacing) with small error margins for the fixed turbine arrangements.

In general, slightly larger errors in the correction predictions occur for large thrust coefficients, well

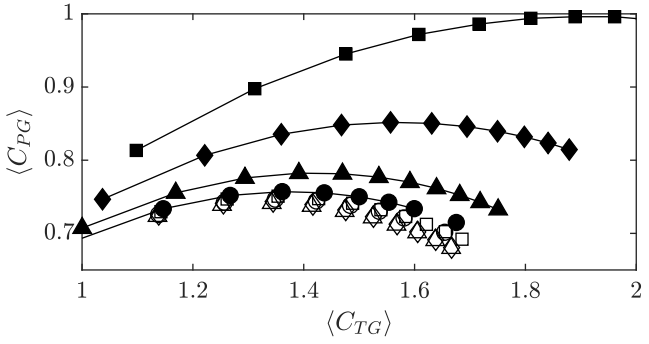

(a) $s/d = 0.1$, $B_L = 0.357$

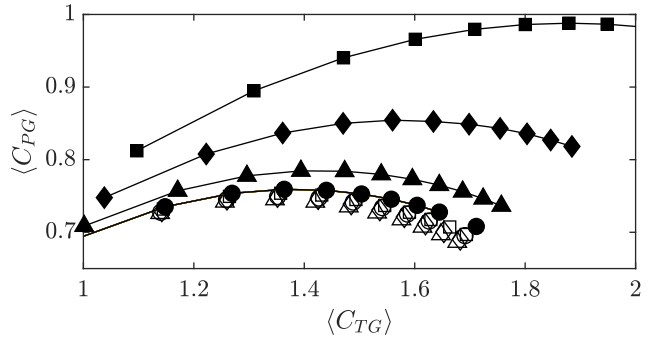

(b) $s/d = 0.25$, $B_L = 0.314$

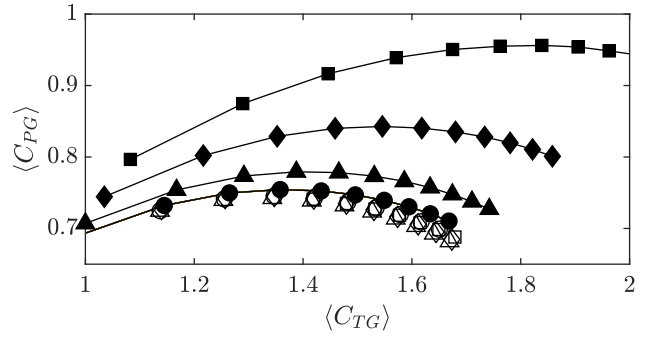

(c) $s/d = 0.5$, $B_L = 0.262$

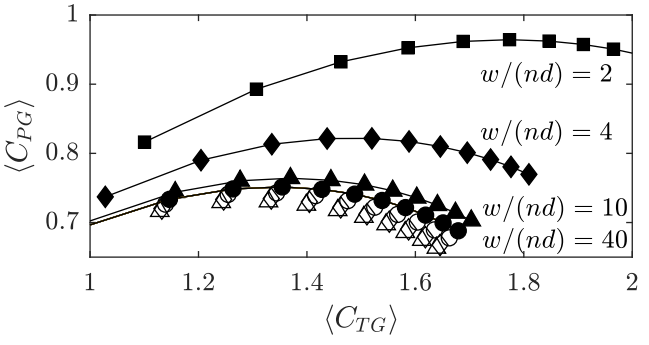

(d) $s/d = 1.0$, $B_L = 0.196$

Fig. 6. Two-scale blockage corrections to the numerical results for the range of local and global blockage ratios presented in Table. II & Table. III. Solid symbols represent simulation results, connected with a line between points for convenience. Hollow symbols represent two-scale blockage corrected results. The channel widths of $w/(nd) = 2$, $w/(nd) = 4$, $w/(nd) = 10$, $w/(nd) = 40$ are represented by squares, diamonds, triangles and circles respectively. For a set tip-to-tip turbine spacing, the corrected curves closely follow one another just below the nearly unblocked simulation case, demonstrating the validity of the proposed correction.

above the peak power point, and for the smallest turbine spacing (i.e. largest local blockage $B_L = 0.196$). These increased errors stem from the limitations of the proposed model. The two-scale theory from which the blockage correction is derived assumes that the device-scale wake mixing takes place much faster than the array-scale flow expansion i.e. that the two-scales are completely separated. This is however only valid when the number of turbines in the fence is sufficiently large. Nishino & Willden [19] developed a model to account for short fences and found that the solutions asymptote to the two-scale theory as the number of turbines in the fence increases. When accounting for finite number of turbine fences, deviation from the two-scale theory depends on the operating conditions, channel and turbine layouts, as well as the numerical mixing assumptions. Correcting the various configurations, particularly at larger disc loadings where the finite fence effect is expected to be of larger significance, is therefore expected to lead to the slightly increased errors observed. Secondly, the validity of the proposed blockage correction is limited in the case of $B_L \approx B_G$, or where $B_A \approx 1$. For example in the limit for $B_A = 1$, it can be shown from the theory in section II-B that the model is only valid for $B_L C_{TG} \leq 1/3$, and therefore breaks down at larger B_L and C_{TG}. This impacts the largest turbine spacing combined with smallest channel width cases for which the correction can no longer be applied. These cases are however typically outside of the area of interest as widely spaced turbines are unlikely to be placed in a co-planar fence configuration in a very narrow channel. In these cases however, existing single-scale blockage corrections are recommended instead.

Nonetheless, the proposed two-scale blockage correction clearly corrects the performance of blocked turbine arrays to free-flow conditions with excellent accuracy across a wide range of disc spacing (local blockage), channel width (global blockage), and operating conditions.

IV. Conclusions

This study proposes a new two-scale blockage correction method for an array of turbines operating in a channel. It extends a two-scale theoretical model [7] for the performance of a row of co-planar turbines partially spanning the width of a tidal channel by developing a relationship between free-flow (unblocked) and blocked flow conditions.

The model is validated by RANS-AD simulations with an array of $n = 8$ turbines across a range of realistic turbine tip-to-tip spacings (local blockage) and channel width (global blockage). The proposed correction shows excellent agreement with the numerical results across a wide range of realistic local and global blockage ratios.

A limitation of the proposed correction is that it relies on the assumption of complete separation between local and array scales, which is only true for a large number of discs in the fence. The correction can therefore be extended on by following the same formulation but with short-fence theory [19] instead to

account for low turbine number fence configurations. An additional extension to the two-scale correction can be to consider the effects of free-surface deformation [4], here assumed negligible.

A particularly useful aspect of the theoretical model is to allow for experimental quantification of the local blockage effect for turbine fences which partially span the width of a tidal channel. While constructive interference effects which exploit the local blockage ratio may be present in both full-scale deployments and reproduced in experiments, the constraints imposed by the dimensions of experimental facilities will likely introduce array, and therefore global, blockage effects as well that would not otherwise be observed at full scale. For instance, doubling the fence length doubles the global blockage, but increases in fence thrust and power cannot be attributed only to the change in global blockage due to non-linear coupling between local and global blockage effects. This correction allows for a decoupling of these two effects, such that the local blockage effect can be isolated and quantified. The blockage corrected results can then for example be combined with models of fence performance in channels with an oscillatory tidal current [20] for a complete understanding of *in-situ* performance.

Acknowledgement

This research was funded in part by D.D.'s EPSRC studentship (grant no. EP/S023801/1), C.R.V.'s UKRI Future Leaders Fellowship (grant no. MR/V02504X/1) and R.H.J.W.'s EPSRC Advanced Fellowship (grant no. EP/R007322/1), and by the EPSRC Supergen ORE Hub (grant no. EP/S000747/1).

References

[1] F. W. Lanchester, "A Contribution to the Theory of Propulsion and the Screw Propeller," *Journal of the American Society for Naval Engineers*, vol. 27, no. 2, pp. 509–510, 1915.

[2] A. Betz, "Das Maximum der theoretisch möglichen Ausnützung des Windes durch Windmotoren," *Zeitschrift für das gesamte Turbinenwesen*, vol. 26, pp. 307–309, 1920.

[3] C. Garrett and P. Cummins, "The efficiency of a turbine in a tidal channel," *Journal of Fluid Mechanics*, vol. 588, pp. 243–251, 2007.

[4] C. Vogel, G. Houlsby, and R. Willden, "Effect of free surface deformation on the extractable power of a finite width turbine array," *Renewable Energy*, vol. 88, pp. 317–324, 2016.

[5] C. R. Vogel, R. H. Willden, and G. T. Houlsby, "Blade element momentum theory for a tidal turbine," *Ocean Engineering*, vol. 169, pp. 215–226, 2018.

[6] D. Coles and T. Walsh, "Mechanisms for reducing the cost of tidal stream energy," in *13th European Wave and Tidal Energy Conference*, 2019, pp. 1–8.

[7] T. Nishino and R. Willden, "The efficiency of an array of tidal turbines partially blocking a wide channel," *Journal of Fluid Mechanics*, vol. 708, pp. 596–606, 2012.

[8] J. McNaughton, B. Cao, A. Nambiar, T. Davey, C. R. Vogel, and R. H. Willden, "Constructive interference effects for tidal turbine arrays," *Journal of Fluid Mechanics*, vol. 943, p. A38, 2022.

[9] F. Zilic de Arcos, G. Tampier, and C. R. Vogel, "Numerical analysis of blockage correction methods for tidal turbines," *Journal of Ocean Engineering and Marine Energy*, vol. 6, no. 2, pp. 183–197, 2020.

[10] H. Ross and B. Polagye, "An experimental assessment of analytical blockage corrections for turbines," *Renewable Energy*, vol. 152, pp. 1328–1341, 2020.

[11] H. Glauert, *Airplane Propellers*. Berlin, Heidelberg: Springer Berlin Heidelberg, 1935, pp. 169–360. [Online]. Available: https://doi.org/10.1007/978-3-642-91487-4_3

[12] M. J. Barnsley and J. F. Wellicome, "Wind tunnel investigation of stall aerodynamics for a 1.0 m horizontal axis rotor," *Journal of Wind Engineering and Industrial Aerodynamics*, vol. 39, pp. 11–21, 1992.

[13] A. Bahaj, A. Molland, J. Chaplin, and W. Batten, "Power and thrust measurements of marine current turbines under various hydrodynamic flow conditions in a cavitation tunnel and a towing tank," *Renewable Energy*, vol. 32, no. 3, pp. 407–426, 2007.

[14] R. Mikkelsen and J. Sørensen, "Modelling of wind tunnel blokage," in *Global Windpower Conference and Exhibition*, 2002, 2002 Global Windpower Conference and Exhibition ; Conference date: 02-04-2002 Through 05-04-2002.

[15] M. J. Werle, "Wind turbine wall-blockage performance corrections," *Journal of Propulsion and Power*, vol. 26, no. 6, pp. 1317–1321, 2010.

[16] G. Houlsby, S. Draper, and M. Oldfield, "Application of linear momentum actuator disc theory to open channel flow," University of Oxford, Tech. Rep. OUEL 2296/08, 2008.

[17] E. Maskell, "A theory of blockage effects on bluff bodies and stalled wings in a closed wind tunnel," HMSO, London, Tech. Rep., 1963.

[18] B. Launder and D. Spalding, "The numerical computation of turbulent flows," *Computer Methods in Applied Mechanics and Engineering*, vol. 3, no. 2, pp. 269–289, 1974.

[19] T. Nishino and R. Willden, "Two-scale dynamics of flow past a partial cross-stream array of tidal turbines," *Journal of Fluid Mechanics*, vol. 730, pp. 220–244, 2013.

[20] D. Dehtyriov, C. Vogel, and R. Willden, "A head-driven model of turbine fence performance," *Journal of Fluid Mechanics*, vol. 956, p. A14, 2023.